Neuroscience 280 (2014) 328–339

CHARACTERIZATION OF SPINAL CORD GLIAL CELLS IN A MODEL OF HINDLIMB UNLOADING IN MICE

Y. A. CHELYSHEV,[a,c] Y. O. MUHAMEDSHINA,[a]* T. V. POVYSHEVA,[c] G. F. SHAYMARDANOVA,[b] A. A. RIZVANOV,[c] M. V. NIGMETZYANOVA,[a] O. V. TIAPKINA,[b] N. I. BONDARENKO,[c] E. E. NIKOLSKIY[a,b,c] AND R. R. ISLAMOV[a]

[a] *Kazan State Medical University, Kazan, Russia*

[b] *Kazan Institute of Biochemistry and Biophysics, Russian Academy of Sciences, Kazan, Russia*

[c] *Kazan (Volga Region) Federal University, Kazan, Russia*

Abstract—Exposure to microgravity has been shown to result in damaging alterations to skeletal muscle, bones, and inner organs. In this study, we investigated the effects of microgravity by using a hindlimb unloading model (HUM) in mice. The characteristics of the lumbar spinal cords of HUM mice 30 days after hindlimb unloading were examined. Morphometric analysis showed reductions of the total area, gray matter, and white matter by 17%, 20%, and 12%, respectively. Myelinated fibers in the white matter showed prominent myelin destruction. Analysis of the number of glial fibrillary acidic protein (GFAP+)/S100 calcium-binding protein B (S100B−), GFAP+/S100B+, and GFAP−/S100B+ astrocytes in the ventral horn (VH), central channel area (CC), dorsal root entry zone (DREZ), main corticospinal tract (CST), and ventral funiculi (VF) showed that the number of GFAP+/S100B− astrocytes was increased in the DREZ and CST of HUM mice. Additionally, GFAP+/S100B+ cell numbers were significantly decreased in the VH and CST but did not differ in the CC or DREZ of HUM mice, as compared with the control. The numbers of GFAP−/S100B+ cells were significantly reduced only in the VH of HUM mice. Moreover, the number of ionized calcium-binding adaptor molecule 1 (Iba1+) microglia cells was significantly increased in the CC and DREZ of HUM mice. In control mice, homeobox protein HoxB8 (HoxB8+) cells were found only in the CC; in contrast, HoxB8+ cells were observed in all studied areas in HUM mice, with the greatest number found in the CC. Genome-wide transcriptome analysis of the lumbar spinal cords of HUM mice showed decreased expression of genes encoding myelin, extracellular matrix, cytoskeleton, and cell adhesion proteins. Real-time polymerase chain reaction (PCR) confirmed reductions in the expression of *mpz*, *pmp2*, *pmp22*, and *prx* genes, which are involved in myelination, as well as decreases in the levels of genes encoding extracellular matrix molecules, including glycoproteins (matrix gla protein (MGP), osteoglycin (OGN), microfibrillar associated protein 5 (MFAP), and collagen, type IV, alpha 1 (COL4A)), proteoglycans (perlecan (heparan sulfate proteoglycan) (HSPG)), and metalloproteinases (lysyl oxidase (LOX)). Thus, our results showed that hindlimb unloading caused decreases in gray and white matter areas, changes in gene expression, alterations in myelination, and phenotypic modifications in glial cells in the lumbar spinal cords of mice.

Key words: hindlimb unloading model, spinal cord, glia, myelin.

INTRODUCTION

The negative effects of long-term microgravity have been well documented, and many organs and limb skeletal muscles have been shown to be particularly vulnerable. Even during the first day of exposure to microgravity, the skeletal muscles responsible for postural control display alterations typical of microgravity locomotion syndrome (MLS) (Caiozzo et al., 1996; Ohira et al., 2002; Kozlovskaya et al., 2007; Fitts et al., 2010). Therefore, elucidation of the mechanisms mediating these effects of microgravity is essential.

Changes in spinal cord neural muscle control have been hypothesized to be responsible for the deleterious influence of microgravity during space trips or in ground-based animal models. In a ground-based model of microgravity (the hindlimb unloading model [HUM]), we previously showed that motor neurons display decreased choline acetyltransferase (ChAT) levels, undergo mild stress changes (upregulation of heat-shock protein [Hsp] 25 and 70), and do not exhibit signs

*Corresponding author. Address: Kazan State Medical University, Butlerov Street 49, Kazan 420012, Russia. Tel: +7-9274307511; fax: +7-843-236-0393.

E-mail address: yanakazmedhist1@rambler.ru (Y. O. Muhamedshina).

Abbreviations: ANOVA, analysis of variance; ANXA3, annexin A3; CC, central canal; COL4A1, collagen, type IV, alpha 1; CST, main corticospinal tract; DHH, desert hedgehog; DREZ, dorsal root entry zone; EM, electron microscopy; GFAP, glial fibrillary acidic protein; HoxB8, homeobox protein HoxB8; HSPG2, perlecan (heparan sulfate proteoglycan 2); HUM, hindlimb unloading model; Iba1, ionized calcium-binding adaptor molecule 1; LOX, lysyl oxidase; MFAP5, Microfibrillar-associated protein 5; MGLAP, matrix Gla protein; MGP, matrix gla protein; MLS, microgravity locomotion syndrome; MPZ, myelin protein zero; OGN, osteoglycin; Olig2, oligodendrocyte transcription factor 2; PBS, phosphate-buffered saline; PCR, polymerase chain reaction; PI3K, phosphoinositol 3-kinase; PLEKHA4, pleckstrin homology domain-containing, family A (phosphoinositide binding-specific) member 4; PMP2, peripheral myelin protein 2; PMP22, peripheral myelin protein 22; PRX, periaxin; RT, room temperature; S100A11, S100 calcium-binding protein A11 (calgizzarin); S100B, S100 calcium-binding protein B; UACA, uveal autoantigen with coiled-coil domains and ankyrin repeats; VF, ventral funiculi; VH, ventral horn.

http://dx.doi.org/10.1016/j.neuroscience.2014.09.004

of apoptosis (negative staining for terminal deoxynucleotidyl transferase dUTP nick end labeling [TUNEL] assays and activated caspase 3) (Islamov et al., 2007, 2011). Such changes are accompanied by atrophy of the hind limb skeletal muscles and increased muscle excitability (Tyapkina et al., 2006).

Astrocytes are the most abundant glial cells and are involved in the metabolic support of neurons. Astrocytes also act as active scavengers of the extracellular milieu, buffering the levels of potassium and glutamate in order to protect neurons against overexcitation (Allaman et al., 2011; Barreto et al., 2011). Astrocytes are very reactive cells and exhibit prominent changes in many brain pathologies. One of the most dramatic changes observed during activation of astrocytes is upregulation of glial fibrillar acidic protein (GFAP), a major constituent of astrocyte-specific intermediate filaments. Moreover, changes in astrocyte function may influence virtually every cellular population in the brain (Sofroniew and Vinters, 2010). In particular, microglia, which are highly sensitive to various perturbations, may influence neurons and macroglial when activated and are therefore of special interest to researchers (Kettenmann et al., 2011). In addition, NG2 cells, which were previously considered astrocytes, comprise a special type of macroglia that act as the main precursors of oligodendrocytes (Trotter et al., 2010). These cells, which are also known as oligodendrocyte precursor cells (OPCs), may be identified by positive oligodendrocyte transcription factor 2 (Olig2) immunolabeling.

In this study, we investigated changes in the lumbar spinal cords of HUM mice after 30 days of hindlimb unloading. We further examined changes in the populations of glial cells in various regions of the spinal cord and evaluated changes in gene expression levels associated with the HUM using gene arrays and real-time polymerase chain reaction (PCR). Electron microscopy (EM) was used to examine the myelin ultrastructure. Our results suggested that changes in the distributions of glial cells may cause an imbalance in skeletal muscle innervation, thereby increasing the risk of MLS.

EXPERIMENTAL PROCEDURES

Experimental animals

Experiments were performed in male C57B/6 mice (weight, 25 ± 3 g each; Pushchino Laboratory, Russia). All animal procedures and care were carried out according to the guidelines of the Kazan State Medical University Animal Care and Use Committee, and experimental protocols were consistent with the recommendations of the Physiological Section of the Russian National Committee on Bioethics. Animals had ad libitum access to food and water and were on a complete and balanced standard laboratory diet. To model microgravity, we used the HUM (Morey-Holton and Globus, 2002) as previously described (Islamov et al., 2011). Briefly, mice (n = 25) were suspended by their tails for 30 days in a special chamber where they could touch the cage floor only with the forelimbs, preventing the hindlimbs from supporting any weight. This method is widely used for studying the effects of microgravity on laboratory animals on Earth and has been approved by the National Aeronautics and Space Administration (NASA) Ames Research Center (ARC) Animal Care and Use Committee as a model for simulating spaceflight.

Histology

Mice were anesthetized with ketamine–xylazine and sacrificed by intracardiac perfusion with 4% paraformaldehyde in phosphate-buffered saline (PBS). Lumbar spinal cords were removed and incubated in a fixative for 12–16 h at 4 °C. After incubation in 15% and 30% sucrose, samples were frozen in liquid nitrogen and embedded in tissue freezing medium (TBS). Frozen cross sections (20 μm) of the lumbar enlargement were prepared with a cryostat Microm HM 560 (Thermo Scientific) and mounted on glass slides.

Morphometric analysis of spinal cord size

Each of twenty transverse sections of the lumbar enlargement was collected for morphometric analysis. Sectioning was started from the point of lumbar spinal cord enlargement both in control and experimental groups of mice. Routine methylene blue staining was used for histological evaluation of the sections and discrimination between gray and white matter.

Images were obtained with microscope (Olympus BX51WI) using a 4× objective equipped with a digital camera (AxioCam MRm, Carl Zeiss). Areas of interest (gray and white matter) were outlined and measured with ImageJ 1.43 (public domain).

Immunofluorescence

Free-floating 20-μm transverse sections obtained with the cryostat were used for immunofluorescence studies. Primary and secondary antibodies and their dilutions are shown in Table 1. For single and double immunofluorescence, sections were first blocked with 10% normal goat serum for 30 min at room temperature (RT) and were then incubated overnight at 4 °C with primary antibodies or in a mixture of primary antibodies raised in different species. For visualization, Alexa Fluor-conjugated secondary antibodies were applied for 1 h at RT. DAPI (Sigma, USA) was used for visualization of nuclei. Blocking serum, primary antibodies, secondary antibodies, and DAPI were applied in 0.2% Triton X-100 in PBS. Sections were then mounted on slides in antiquenching medium (Vectashield, Vector Labs, USA). To control the specificity of immunostaining, primary antibodies were omitted and substituted with normal serum. Slides were viewed using an LSM 510-Meta microscope (Carl Zeiss, Germany) with a 40× objective and a Leica SP-5 confocal microscope with a 40× objective.

Five areas were selected for quantitative immunohistochemical evaluation of glial cells: the ventral horn (VH), analyzed as gray matter containing motor neurons; the main corticospinal tract (CST) and ventral funiculi (VF), analyzed as parts of the

Table 1. Primary and secondary antibodies used in immunofluorescent staining

Antibody	Host	Dilution	Source
GFAP	Mouse	1:200	Santa Cruz
S100B	Rabbit	1:1 200	Santa Cruz
Iba1	Rabbit	1:200	Biocare
Hoxb8	Rabbit	1:100	Abcam
Anti-rabbit IgG conjugated with Alexa 555	Goat	1:150	Invitrogen
Anti-mouse IgG conjugated with Alexa 647	Goat	1:150	Invitrogen

pyramidal.tract originating from cortex motor neurons; the area around the central canal (CC), analyzed as a neurogenic zone of the spinal canal; and the dorsal root entry zone (DREZ), analyzed as a border between the central and peripheral nervous systems.

Quantitative immunohistochemical analysis

The numbers of GFAP-, S100 calcium-binding protein B (S100B)-, ionized calcium-binding adaptor molecule 1 (Iba1)-, and homeobox protein HoxB8 (HoxB8)-immunopositive cells were quantified in the above-mentioned areas in merged images captured using a 40× objective from five adjacent optical slices (pixel resolution, 512 × 512; observed area, 0.05 mm^2; acquisition distance, 0.5 μm). Only cells with clearly outlined nuclei were evaluated.

EM

After initial fixation by perfusion as described above, the lumbar spinal cord was cut into small pieces. These small pieces were further fixed in 2.5% glutaraldehyde for 12 h at 4 °C). After post-fixation with 1% osmium tetroxide and dehydration, pieces were embedded in Epon-Araldite. Ultrathin sections (Ultracut LKB III, Bromma, Sweden) were contrasted with uranyl acetate and lead citrate and examined with a JEM-1200 electron microscope.

Microarray analysis

Total RNA was extracted from the lumbar enlargement of the spinal cord using an RNAeasy kit (Qiagen, Valencia, CA, USA) according to the manufacturer's instructions. RNA content was measured with a NanoDrop Spectrophotometer (A260/280; model 2000, Thermo Scientific, USA). RNA was further characterized using chips from an Agilent RNA 6000 Nano Kit (Agilent, USA) in accordance with the manufacturer's recommendations. Amplification of 400 ng of extracted RNA was performed with an Illumina TotalPrep RNA Amplification Kit (Ambion, USA). Genomic analysis of mRNA expression was performed with Illumina MouseRef-8 v.2 Expression BeadChips, which allowed us to examine eight samples simultaneously in one chip and to obtain information on the expression of 25,697 transcripts annotated in the RefSeq database representing 16,948 unique genes from the NCBI RefSeq database (Build 36.2, Release 22) (Pruitt et al., 2007). Data were analyzed with GenomeStudio software (Illumina, USA) in Microsoft Office Excel (Microsoft, Redmond, WA, USA).

Real-time PCR

Gene expression was investigated with real-time reverse transcription PCR (qRT-PCR) using an iCycler iQ real-time PCR Detection System (Bio-Rad, Hercules, CA, USA). Total RNA was extracted and evaluated as described above. Both reverse transcriptase and DNA polymerase were added during the initial reaction setup, and the thermal cycler was programed to perform the reverse transcription step, immediately followed by the thermal cycling program. TaqMan primers and probes were designed using PrimerExpress (Applied Biosystems, USA) software (Table 2). Real-time PCR

Table 2. Primers and probes for RT-PCR

Type of oligonucleotide	Nucleotide sequence
rmMpz-TM-S	TCGCAAAGATGAGCAGAG
rmMpz-TM-A	GGCCCATCATGTTCTTGA
Mpz-TMpr*	CCAGTAGAACCAGCCTCAAGAAC
Pmp22-TM-S	GTGCTAGTGTTGCTCTTC
Pmp22-TM-A	GGATGTGGTACAGTTCTG
Pmp22-TMpr*	CTCCACCATCGTCAGCCAAT
mPmp2-TM-S	TCACCATTAGAACGGAAAG
mPmp2-TM-A	TCTCCTTATGGCTGTCTC
Pmp2-TMpr*	CCACTTCTGCACTTGCTTCA
mPrx-TM-S	GAAGCCAAAGTAGTCAAGG
mPrx-TM-A	GGGTTCCAGGAGAGAAAG
Prx-TMpr*	CAGACTTCGAATGCCCACCTT
mMgp-TM-S	CATGGTCTACGGCTACAA
mMgp-TM-A	GTCTGTATACTTCAGTAATGCTA
Mgp-TMpr*	ACAACCGCTACTTCAGGCAG
rmOgn-TM-S	TCCTGATGAGAAAAGTCTTC
rmOgn-TM-A	GGTACAGCATCAATGTCA
Ogn-TMpr*	CTTCTTCACAGTAGACAGAGCCAC
Mfap5-TM-S	GGATGAGAAGTTTGCTTG
Mfap5-TM-A	GGGAACAGATCTCATTATTG
Mfap5-TMpr*	ACTGTACTCTGTCCATCGGC
Col4a1TM-S	CTTCCAAGGACCAAAAGG
Col4a1TM-A	GACCCTTTTCTCCTGTTG
Col4a1TMpr*	TTCCTTAACTTGTGCCTGTCCA
mHspg2TM-S	CGCATTGAATCCTCGTCA
mHspg2TM-A	GCTTGTACCAGGTGATGG
Hspg2-TMpr*	TACTCTGGACCTGAACTGCCT
mLox-TM-S	GAGTCCTGGATGTTATGA
mLox-TM-A	CACTGACCTTTAGAATGTAG
Lox-TMpr*	ACATCTGTAATATCAATCCACTGGCA

* TaqMan probes for Real-Time PCR contained 5'-end FAM fluorescent.

2.5× premix was purchased from Syntol (Moscow, Russia) and used according to manufacturer's instructions. PCR thermal cycling conditions: 95 °C for 15 s, 60 °C for 50 s (45 cycles). The specificity of the PCR products was verified by gel analysis, and products were shown to consist of only a single band. Data were normalized to the expression of the 18S rRNA housekeeping gene.

Statistical analysis

Data are expressed as mean ± standard errors of the means (SEMs). Student's *t*-tests or a one-way analysis of variance (ANOVA) for multiple groups with Tukey's test were used as appropriate. Differences with *P*-values of less than 0.05 were considered significant.

RESULTS

Atrophy of the spinal cord in HUM mice

Morphometric analysis of transverse sections of lumbar enlargements showed significant decreases in the cross-sectional areas of the spinal cord in HUM mice after 30 days of hindlimb unloading. Moreover, the total area of the spinal cord was significantly reduced in transverse sections from HUM mice ($2.78 \pm 0.02\ mm^2$ in the control vs. $2.31 \pm 0.06\ mm^2$ in HUM mice, $p < 0.05$, $n = 6$ in both groups), with a greater decrease observed in gray matter than in white matter (20.4% vs. 12.7%, respectively, $p < 0.05$; Fig. 1).

Immunofluorescence analysis of glial cells

Astrocytes. Next, we evaluated the distributions of different populations of astrocytes. GFAP, a specific marker of astrocytes, and S100B, which is expressed in oligodendrocytes and NG2 cells, were used for analysis of astrocytes (Hachem et al., 2005).

In control mice, only a portion of GFAP+ astrocytes expressed S100B (~39%) in gray matter, while virtually all GFAP+ astrocytes co-expressed S100B in the white matter of the CST. Therefore, we quantified the numbers of GFAP+/S100B−, GFAP+/S100B+, and GFAP−/S100B+ cells. Numbers of astrocytes with different immunohistochemical profiles were differentially changed in studied areas of gray and white matter in HUM mice (Fig. 2).

GFAP+/S100B− cells. In the VH (Fig. 2, A1–A6) and CC (Fig. 2, B1–B6), there was a significant (approximately twofold) decrease in the numbers of GFAP+/S100B− astrocytes in HUM mice (Fig. 2). In the CST (Fig. 2, C1–C6), GFAP+/S100B− astrocytes were absent in control mice, but were observed following hindlimb unloading. In the DREZ, the number of GFAP+/S100B− astrocytes was increased in HUM mice in comparison with control mice (Fig. 2, D1–D6).

GFAP+/S100B+ cells. Numbers of GFAP+/S100B+ cells were significantly reduced in the VH and CST of HUM mice, but did not differ in the CC and DREZ in comparison with the control (Fig. 2).

GFAP−/S100B+ cells. Numbers of GFAP−/S100B+ cells were significantly reduced only in the VH of HUM mice (Fig. 2, A4–A6).

These data indicated that the majority of reductions in astrocyte numbers occurred in the gray matter of the VH, where motor neurons reside.

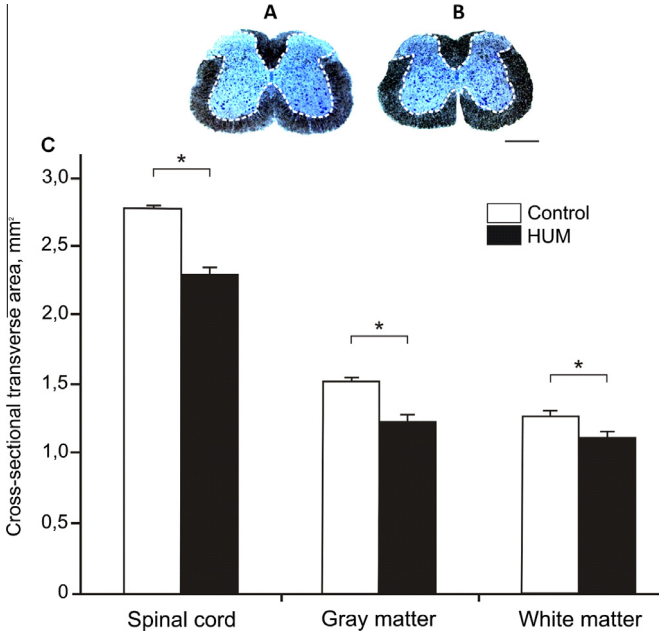

Fig. 1. The cross-sectional area of the lumbar spinal cord was decreased in HUM mice after 30 days. A, B – Representative images of the spinal cord in control (A) and HUM (B) mice. Scale bar = 1 mm. C – Measurement of the areas of the whole spinal cord, white matter, and gray matter. *$P < 0.05$, Student's *t*-test.

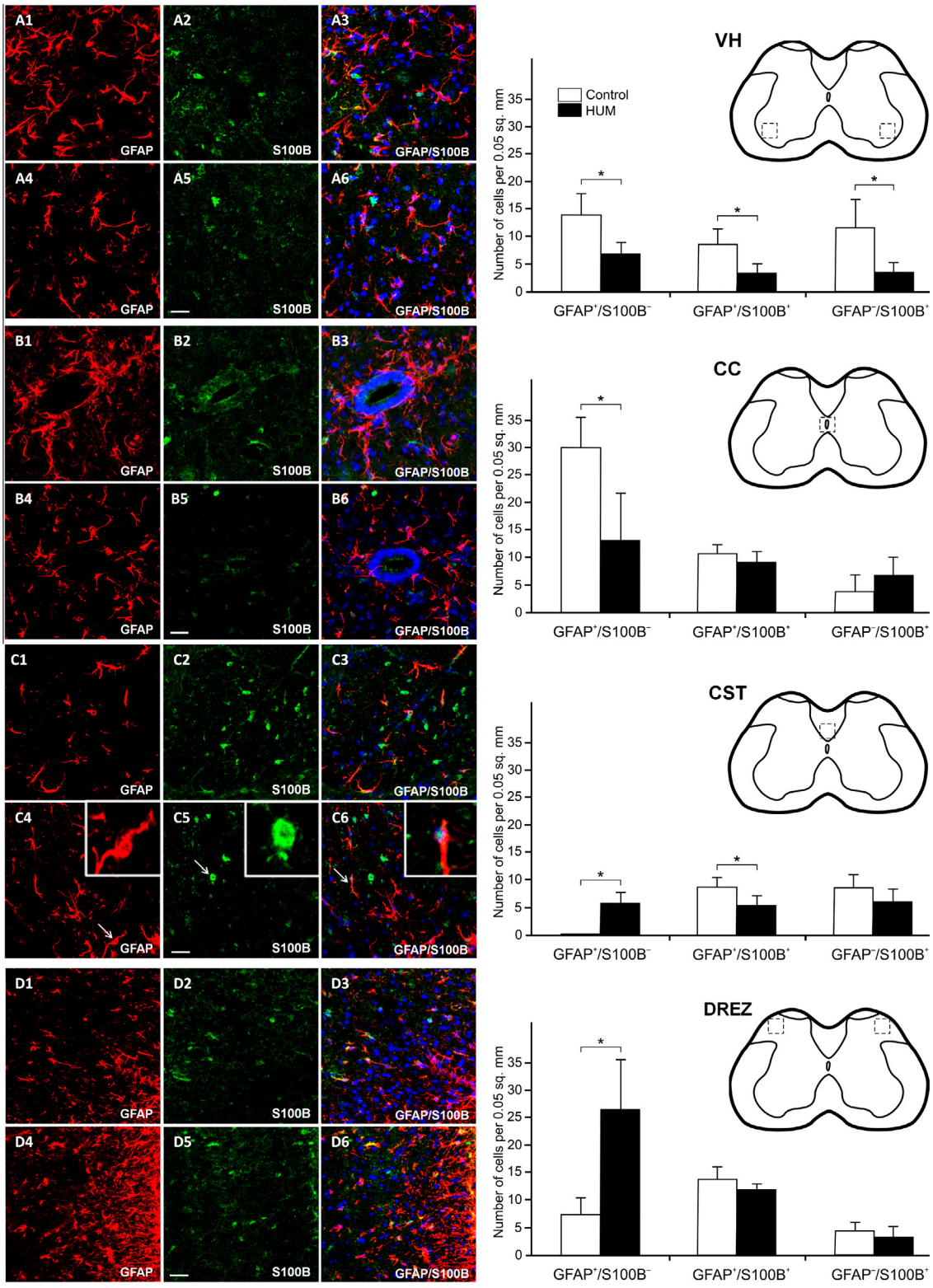

Fig. 2. Differential changes in the expression of GFAP (red) and S100 (green) in the lumbar spinal cords of HUM mice after 30 days. (A1–A6) Ventral horn (VH), (A1–A3) control, (A4–A6) HUM. (B1–B6) Central canal (CC), (B1–B3) control, (B4–B6) HUM. (C1–C6) Corticospinal tract (CST), (C1–C3) control, (C4–C6) HUM. GFAP+/S100B−, S100B+/GFAP−, GFAP+/S100B+ cells are marked with arrows in C4, C5, and C6 and are shown enlarged in boxed areas, respectively. (D1–D6) Dorsal root entry zone (DREZ), (D1–D3) control, (D4–D6) HUM. Nuclei are counterstained with DAPI. Confocal microscopy images are shown. Each image is shown as merged (right panel of images) and separate red and green channels. Scale bars = 20 μm. The right panel of diagrams shows statistical evaluation of the numbers of GFAP+, S100B+, and GFAP+/S100B+ cells in different areas. $^{*}P < 0.05$, Student's *t*-test.

Oligodendroglial cells. To detect oligodendroglial cells, we used Olig2, a marker of mature oligodendrocytes and NG2 cells. In control mice, Olig2+ cells were distributed unequally in the spinal cord, with maximal concentrations in the CST and VH; fewer Olig2+ cells were observed in the DREZ and CC (Fig. 3).

In HUM mice, the number of Olig2+ cells was significantly increased in every studied area, except the CST (Fig. 3). A particularly dramatic increase in the number of Olig2+ cells was found in the DREZ of HUM mice (Fig. 3).

Microglia. Iba1 is a marker of microglial cells that detects both quiescent and reactive microglial cells. In control mice, Iba1+ microglia homogeneously occupied every studied area in the spinal cord. The number of microglial cells in the CST (2.2 ± 0.99 [control] vs. 1.9 ± 0.86 [HUM]), VF (1.6 ± 0.72 [control] vs. 2.1 ± 0.64 [HUM]), and VH (2.7 ± 0.96 [control] vs. 2.3 ± 0.92 [HUM]) did not differ between control and HUM mice. In HUM mice, the number of Iba1+ cells increased significantly in the DREZ (7.1 ± 0.91 [control] vs. 9.1 ± 1.51 [HUM]) and CC (8.1 ± 0.71 [control] vs. 24.1 ± 0.45 [HUM]) (Fig. 4). Notably, in HUM mice, Iba1 immunostaining showed cells with larger, more arborized processes compared with control mice (Fig. 4), indicating significant structural remodeling in microglia.

HoxB8 was used as a marker of bone marrow-derived macrophages, which exhibit many features of resident microglia (Chen et al., 2010). In control mice, HoxB8+ cells were found only in the CC, where they constituted about half of Iba1+ cells (3.7 ± 0.06 vs. 7.4 ± 0.88, respectively). In HUM mice, HoxB8+ cells appeared in every studied area, with the greatest increase observed in the CC (Fig. 4). HoxB8+ cells appear in large numbers in DREZ of HUM mice. In HUM mice, precious single HoxB8+ cells were revealed in the CST, VF и VH but statistically reliable difference was not registered compared with control mice.

In HUM mice, the increase in the number of microglial cells was accompanied by an increase in the number of GFAP+/S100B− cells in DREZ; however, the number of GFAP+/S100B− cells decreased in the CC. A positive correlation can therefore be inferred between the number of Olig2+ and microglial cells in the same experimental group of mice.

Changes in myelinated fibers in lateral columns

EM analysis of the myelinated fibers in the lateral columns showed dramatic alterations in many myelinated fibers in mice after hindlimb unloading (Fig. 5). Some fibers lost

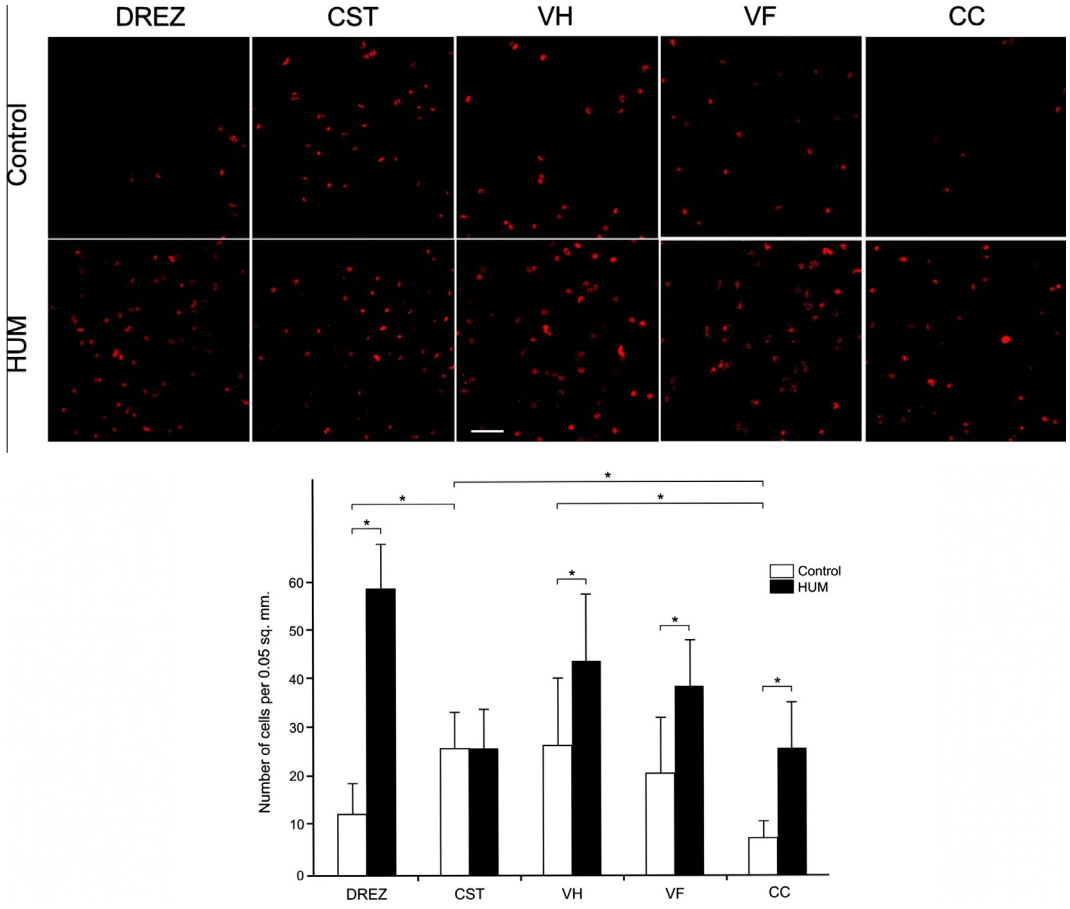

Fig. 3. Increased numbers of Olig2+ cells were observed in the lumbar spinal cords of HUM mice. The upper panel shows representative images of the spinal cord in control and experimental mice. Confocal microscopy images are shown. Scale bar = 20 μm. The diagram shows quantitative evaluation of Olig2+ cells in different areas of the spinal cord. $^{*}P < 0.05$, one-way ANOVA.

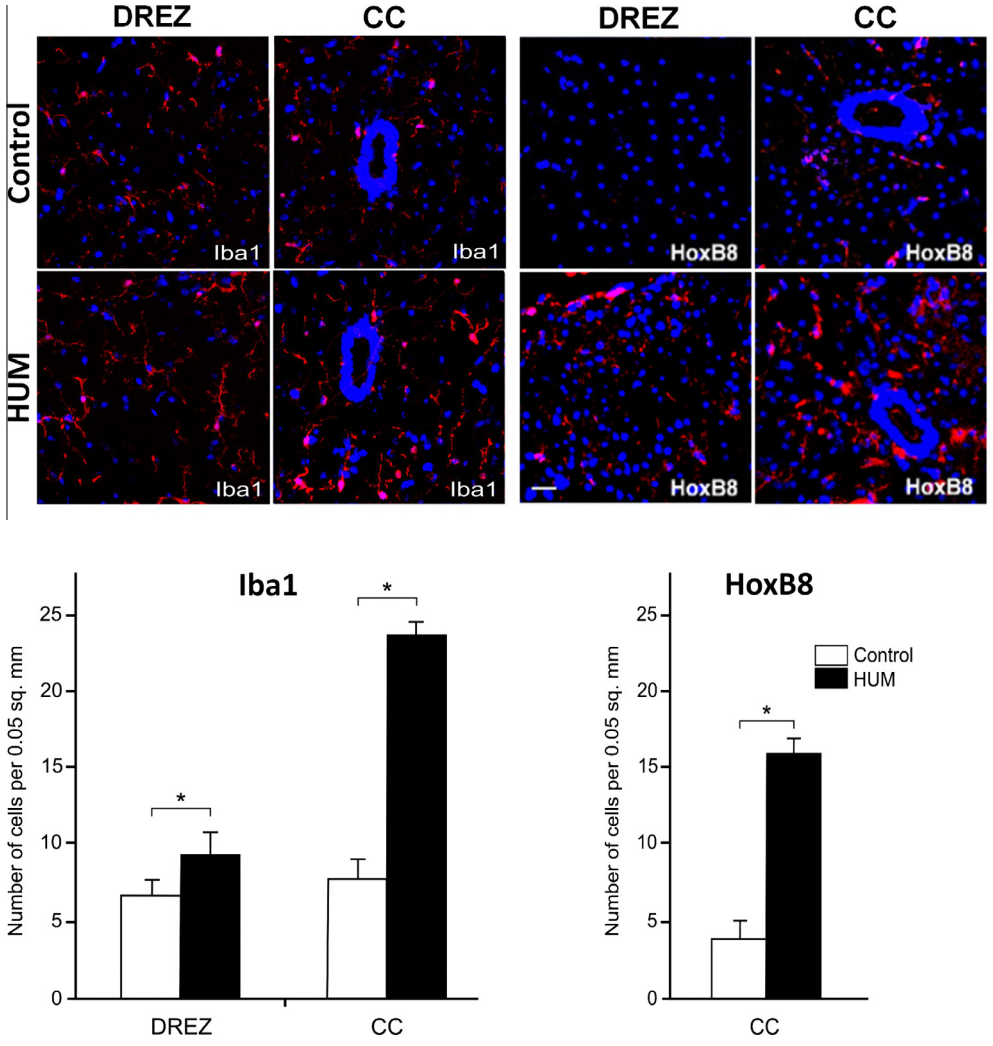

Fig. 4. Microglia were activated in the lumbar spinal cords of HUM mice. The upper panel of images shows the numbers of Iba1+ and HoxB8+ cells in different regions of the spinal cord. Nuclei were counterstained with DAPI. Confocal microscopy images are shown. Scale bar = 20 μm. *$P < 0.05$, Student's *t*-test.

the regular arrangement of myelin lamellae and contained areas of lamellae dissociation and vacuolization. Vacuole-like cavities of different sizes were often found between the myelin sheath and axons. In general, myelinated fibers lost their oval shape, acquired a more angular profile, and appeared shrunken. Many axons had increased electron densities in the cytosol and in damaged regions, similar to autophagosomes.

Analysis of changes in gene expression in the lumbar spines of HUM mice

Microarray analysis. Of the 25,697 genes analyzed by microarray, 37 were downregulated, while only one (*CNNM2*, encoding a plasma membrane transporter for Mg^{2+}) was upregulated in HUM mice (Table 3). Significant decreases were observed in the expression levels of genes encoding myelin-associated proteins (e.g., myelin protein zero (MPZ), peripheral myelin protein 2 (PMP2), peripheral myelin protein 22 (PMP22), and periaxin (PRX)), extracellular proteins (e.g., microfibrillar-associated protein 5 (MFAP5), matrix Gla protein (MGLAP), osteoglycin (OGN), collagen, type IV, alpha 1 (COL4A1), perlecan (heparan sulfate proteoglycan 2) (HSPG2), and lysyl oxidase (LOX)), intracellular signaling pathways (e.g., pleckstrin homology domain-containing, family A (phosphoinositide-binding specific) member 4 (PLEKHA4), S100 calcium-binding protein A11 (calgizzarin) (S100A11), annexin A3 (ANXA3), and uveal autoantigen with coiled-coil domains and ankyrin repeats (UACA)), and growth and morphogenetic factors (e.g., IGF2, IGFBP6, IGFBP7, and desert hedgehog (DHH)).

qRT-PCR. Real-time PCR was used to confirm the results of the gene expression microarray. Consistent with the above results, levels of myelin mRNAs (*mpz*, *pmp2*, *pmp22*, and *prx*) were significantly reduced in HUM mice (Fig. 6). A particularly dramatic decrease was observed for *pmp2* expression (Fig. 6).

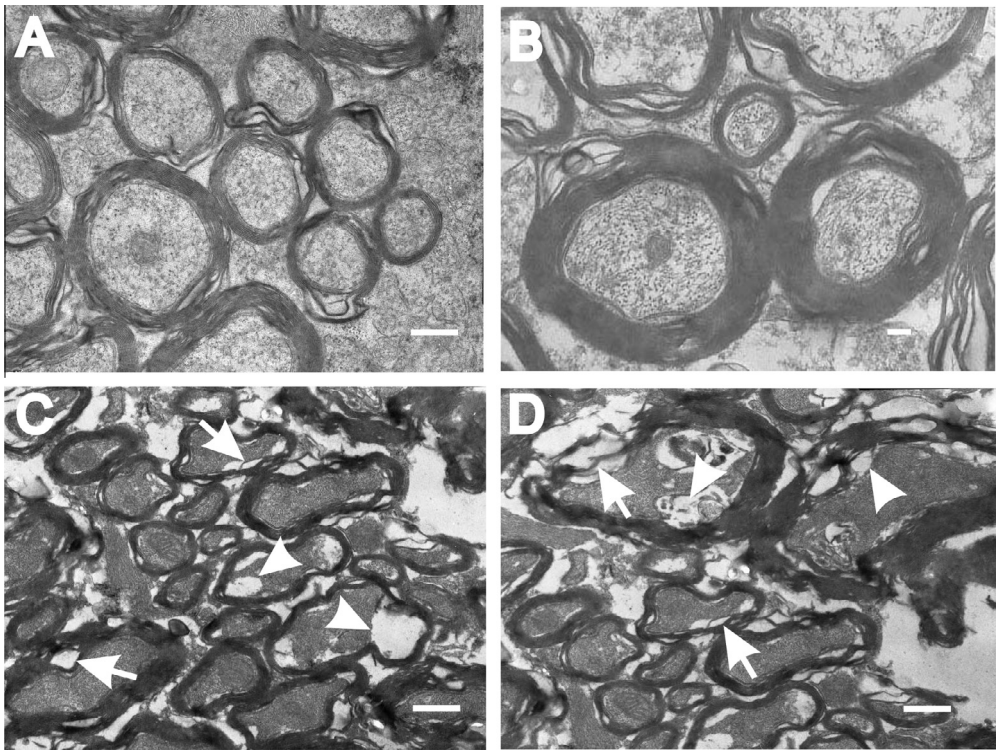

Fig. 5. Electron micrographs of the lateral columns of the lumbar spinal cords from control mice (A, B) and HUM mice (C, D). Note dissociation of myelin sheaths (arrows) and vacuole-like cavities between myelin and axons (arrowheads). Scale bars = A, C, and D, 500 nm; B, 200 nm.

In addition to the above-mentioned genes, significant reductions were detected in mRNA levels of transcripts encoding extracellular proteins, such as glycoproteins and proteoglycans (MGP, OGN, MFAP, COL4A, and HSPG) and metalloproteins (LOX; Fig. 6).

DISCUSSION

In this study, we characterized cellular and molecular changes in the lumbar spines of mice after 30 days of hindlimb unloading. Our data show dramatic changes in cell distributions and gene expression in HUM mice, suggesting important roles for specific genes and cell types in mediating MLS. Interestingly, we observed a decrease in the total area, gray matter area, and white matter area after 30 days of hindlimb unloading. These changes were associated with decreased numbers of astrocytes and changes in the composition of the extracellular milieu. Additionally, microarray and qRT-PCR analyses showed significant downregulation of genes encoding extracellular glycoproteins and proteoglycans, including hyaluronan, which is the main extracellular component required for maintenance of water homeostasis (Laurent et al., 1996). Reductions in these proteins, primarily due to the functions of astrocytes, may lead to decreases in the area of the extracellular space because such glycoproteins and proteoglycans function to hydrate the cellular environment, which regulates the activity of signaling molecules by facilitating binding interactions in the extracellular matrix protein network (Badylak et al., 2009). Taken together, our data suggest that changes in the volumes of spinal cord results from structural changes in the myelin envelope, which reflect downregulation of genes encoding myelin proteins by oligodendrocytes, as well as structural changes in white and gray matter as result of downregulation of genes encoding extracellular glycoproteins and proteoglycans by astrocytes.

Astrocyte loss may result from many deleterious factors, including changes in neuronal (stress reaction [Islamov et al., 2011]), microglial, and vascular cells. Reaction of microglial cells was also observed in the current study. Notably, astrocyte loss is not associated with death of motor neurons in the VH (Islamov et al., 2011). Previous studies have also shown that microgravity has deleterious effects on the astrocyte cytoskeleton, including alteration of GFAP filaments, both *in vitro* and *vivo* (Uva et al., 2002; Nguon et al., 2004). Consistent with this, we observed decreased GFAP immunoexpression in astrocytes in VH and CC of the lumbar spinal cord in HUM mice, reflecting changes in the cytoskeletons of glial cells. These changes may constitute the structural changes affecting signaling processes and intercellular communication between astrocytes and neurons.

Another marker of astrocytes is S100B, a Ca^{2+}-binding protein of the EF-hand type, which has been shown to have multiple functions in various intracellular pathways (Donato et al., 2013). S100B may influence the aggregation/disaggregation of GFAP intermediate filaments due to direct interactions with Src kinase and subsequent activation of phosphoinositol 3-kinase (PI3K)/Akt and PI3K/RhoA pathways (Brozzi et al., 2009). In our study, the number of

Table 3. Gene expression analysis using MouseRef-8 gene expression array (Illumina). HUM – mice with hindlimb unloading model ($n = 4$). Control – mice without any treatment ($n = 4$). Data presented as average gene expression level ± standard deviation (M ± SD). Control/HUN – ratio of gene expression level in control mice relative to gene expression level in experimental group. P – significance level

Gene	GenBank no.	Gene name	HUM	Control	Control/HUM	P
mpz	NM_008623.2	Myelin protein zero	154.3 ± 97.8	1144.0 ± 261.1	7.4	< 0.01
pmp22	NM_008885.1	Peripheral myelin protein 22	190.1 ± 62.3	824.4 ± 199.3	4.3	< 0.01
plekha4	NM_148927.1	Pleckstrin homology domain-containing, family A (phosphoinositide-binding specific) member 4	103.9 ± 30.6	450.1 ± 174.4	4.3	0.01
pmp2	NM_001030305.2	Peripheral myelin protein 2	86.5 ± 32.1	325.4 ± 128.5	3.8	0.01
mfap5	NM_015776	Microfibrillar-associated protein 5	68.2 ± 8.1*	191.3 ± 33.4	2.8	< 0.01
dhh	NM_007857	Desert hedgehog	81.6 ± 7.5	224.8 ± 33.9	2.8	< 0.01
ogn	NM_008760.2	Osteoglycin	76.9 ± 10.5*	207.7 ± 39.7	2.7	< 0.01
igf2	NM_010514.1	Insulin-like growth factor 2 (somatomedin A)	340.7 ± 64.2	884.9 ± 442.1	2.6	0.05
mglap	NM_008597.2	Matrix Gla protein	155.9 ± 17.5	329.4 ± 117.1	2.1	0.03
uaca	NM_028283	Uveal autoantigen with coiled-coil domains and ankyrin repeats	169.2 ± 26.2	346.2 ± 93.8	2.0	0.01
cd9	NM_007657.2	CD9 molecule	353.2 ± 69.6	704.8 ± 127.0	2.0	0.01
cldn19	NM_001038590.1	Claudin 19	69.1 ± 8.4*	133.8 ± 42.9	1.9	0.03
drp2	NM_010078.1	Dystrophin-related protein 2	102.5 ± 8.3	196.3 ± 38.0	1.9	< 0.01
vim	NM_011701.3	Vimentin	143.9 ± 15.9	275.1 ± 84.7	1.9	0.03
prx	NM_198048.1	Periaxin	75.0 ± 10.7*	142.0 ± 24.4	1.9	< 0.01
smtn	NM_013870.1	Smoothelin	89.2 ± 7.0	166.6 ± 26.0	1.9	< 0.01
col4a1	NM_009931.1	Collagen, type IV, alpha 1	120.3 ± 7.4	206.6 ± 18.1	1.7	< 0.01
hspg2	NM_008305.2	Heparan sulfate proteoglycan 2	78.3 ± 3.5*	133.6 ± 20.7	1.7	< 0.01
spon2	NM_133903.2	Spondin 2, extracellular matrix protein	88.0 ± 8.7	149.2 ± 43.6	1.7	0.04
s100a11	NM_016740.3	S100 calcium-binding protein A11	143.9 ± 26.6	243.7 ± 56.8	1.7	0.03
igfbp6	NM_008344.1	Insulin-like growth factor-binding protein 6	73.3 ± 3.6*	123.0 ± 39.1	1.7	0.05
plekha4	NM_148927.1	Pleckstrin homology domain-containing, family A (phosphoinositide binding-specific) member 4	69.0 ± 1.6*	109.8 ± 13.6	1.6	< 0.01
anxa3	NM_013470.1	Annexin A3	186.7 ± 16.0	296.2 ± 19.6	1.6	< 0.01
smtn	NM_013870.1	Smoothelin	74.9 ± 3.3*	118.1 ± 22.3	1.6	0.01
igfbp7	NM_008048.1	Insulin-like growth factor binding protein 7	120.6 ± 14.2	184.7 ± 44.0	1.5	0.04
prx	NM_019412.1	Periaxin	65.6 ± 3.4*	99.3 ± 7.4	1.5	< 0.01
lox	NM_010728.1	Lysyl oxidase	64.6 ± 6.1*	97.1 ± 15.5	1.5	0.01
cnnm2	NM_033569.1	Cyclin M2	266.5 ± 17.4	141.9 ± 21.4	0.5	< 0.01

* mRNA expression at background level of detection.

GFAP+ astrocytes expressing S100B protein in the CST and VH was decreased following hindlimb unloading. We found increased numbers of GFAP+/S100B− cells and decreased number of GFAP+/S100B+ cells. The changes in numbers of GFAP+ astrocytes reflected the changes in S100B protein expression in GFAP+ astrocytes. In this study, we observed increased numbers of Olig2+ cells in virtually all zones of the spinal cord, especially the DREZ and CC, in HUM mice. The basic helix-loop-helix (bHLH) transcription factor Olig2 plays a key role in regulating transcription during the genesis of motoneurons and oligodendrocytes within the ventral part of the spinal cord. Like other helix-loop-helix transcription factors, such as MyoD and NeuroD2, Olig2 lacks a protein transduction domain, but can still penetrate cell membranes (Mie et al., 2012), allowing internalization of this transcription factor into cells and facilitating cell differentiation. This effect of Olig2 on oligodendrocytes and their precursors may have implications for the function of this protein in the damage induced in the HUM. Consistent with this, Olig2+ cells are associated with substantial increases in the numbers of NG2 progenitors; Olig2+ NG2 cells display multipotent properties and generate oligodendrocytes throughout the central nervous system. Moreover, NG2 cells may be activated in response to oligodendrocyte damage. However, it is unclear whether NG2 cells differentiate into mature oligodendrocytes. In addition to its association with NG2 cells, Olig2 was shown to form a complex with another transcription factor from the Wnt signaling pathway in precursors of oligodendrocytes in a model of remyelination in mice (Fu et al., 2012), supporting its role in maintaining the myelin sheath in the spinal cords of adult mice. Further studies are required to elucidate the details of Olig2-mediated mechanisms in these cells.

In our study, we found significant decreases in the expression of several mRNAs encoding myelin-associated proteins in HUM mice using both microarray analysis and qRT-PCR. These peripheral myelin proteins are expressed in the central nervous system in small amounts (DeArmond et al., 1980; Trapp et al., 1983; Hunter et al., 2005).

As a sensitive indicator of perturbations within the nervous system, activated microglia indicated abnormalities in the spinal cords of HUM mice. Activation of microglial cells was observed, particularly in the DREZ and CC. This region also showed a 1.6-fold increase in the number of Ibal+ cells in HUM mice compared with control mice. In addition to Iba1, HoxB8, a homeobox protein, can also be used as a marker of microglia, but indicates the specific population

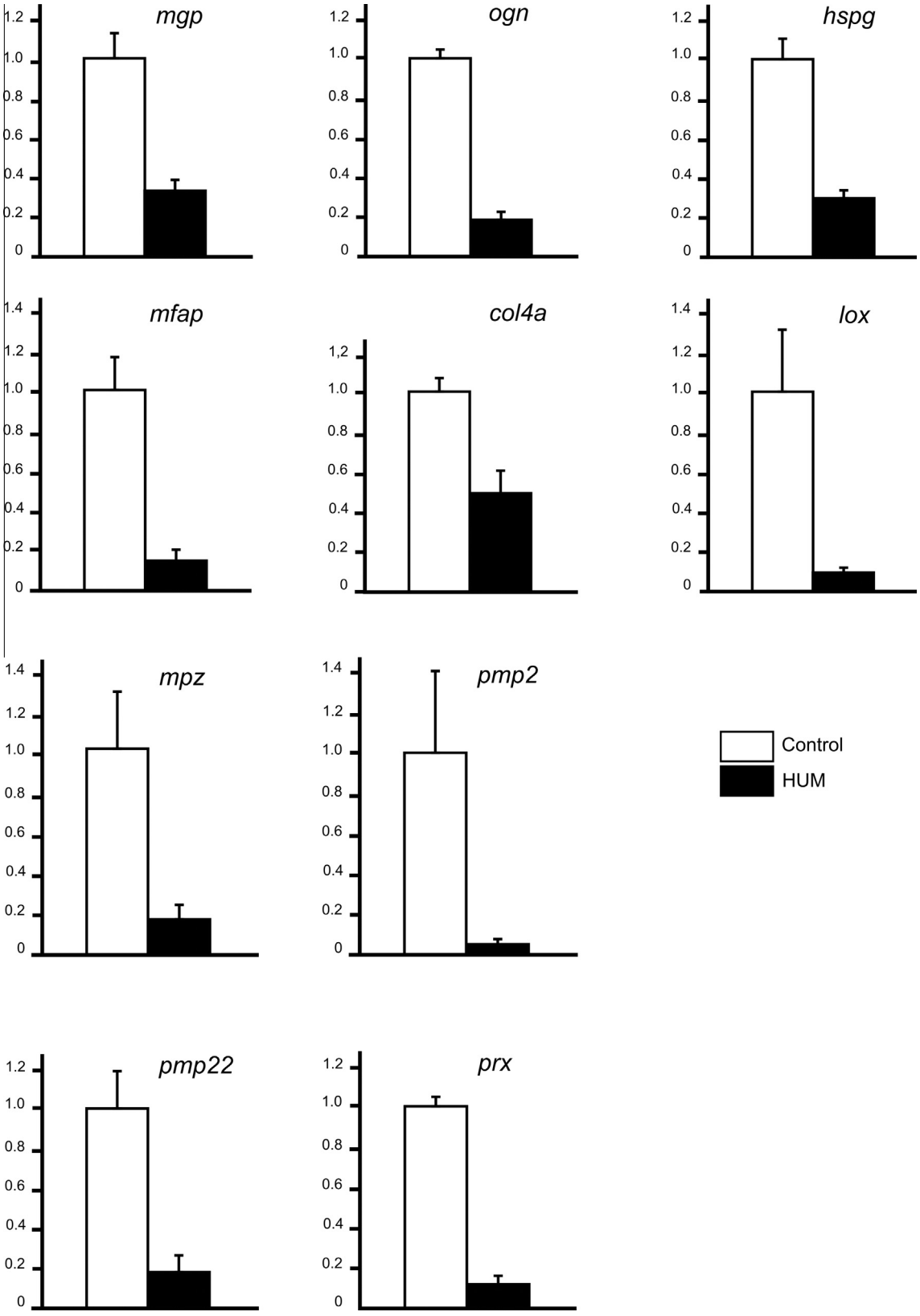

Fig. 6. mRNA expression levels of genes encoding myelin (*mpz*, *pmp2*, *pmp22*, and *prx*) and extracellular matrix proteins (*mgp*, *ogn*, *hspg*, *mfap*, *col4a*, and *lox*) in HUM mice after 30 days of hindlimb unloading. Quantification was performed using real-time PCR with normalization to 18S rRNA levels. $p < 0.05$, $n = 3$ for all comparisons of gene expression levels between HUM and control mice.

of microglia originating from the bone marrow (Chen et al., 2010). *HoxB* genes are expressed actively in the dorsal part of the spinal cord. Decreases in the number and organization of neurons the dorsal horns are observed in mice with *HoxB8* gene mutations, leading to defects in perception, primarily nociception, and flawed behavioral reactions, e.g., excessive grooming (Holstege et al., 2008; Schlegelmilch et al., 2011). The spinal cords of intact mice showed HoxB8+ cells only in the CC, where they constituted a third of all Iba1+ cells of microglia; these cells also appeared in the CST, VH, and DREZ of HUM mice, with the greatest number of HoxB8+ cells observed in the DREZ zone. These data confirmed that there was a heterogeneous population of microglia in the spinal cord. Additionally, the change in the number of HoxB8+ cells in DREZ may influence the behavior of astrocytes linked to the development of hypogravitation syndrome. Activated microglial cells may transform from a process-bearing (ramified) morphology to an ameboid shape. Microglia are activated in response to brain injuries and immunological stimuli to undergo dramatic alterations in morphology, changing from resting, ramified microglia into activated, ameboid microglia (Kreutzberg, 1996). In contrast to the resting microglial cells, classically activated microglial cells are characterized by process retraction, ameboid morphology development, cell body migration, increased phagocytic ability (phagocytic marker CD11b), and increased expression of several receptors of pro-inflammatory signals (TGFβR, IL-4R, IL-6R, and IL-10R) and other molecules. In HUM mice, we found a high number of arborized microglial cells, which does not fit the classical view of the transition from resting microglial cells to reactive microglial cells. However, Morrison and Filosa (2013) demonstrated that microglial activation after injury includes both increased and decreased cell ramification. In HUM mice, ramification of microglial cells is a sign of morphological transformation, which may reflect the increased communication between microglial cells and astrocytes, and the hyper-ramification may include process-directed phagocytosis (Wake et al., 2009) and neurotransmitter modulation (Tremblay et al., 2010).

However, our data did not show a significant correlation between levels of microglia activation and changes in other studied macroglial cell types. HoxB8+ cells are thought to represent blood-derived macrophages (Chen et al., 2010), and their appearance might represent mild leakage of the blood–brain barrier. Although intracranial blood flow alterations are generally believed to occur following exposure to microgravity (Taylor et al., 2013), development and/or the levels of edema remain controversial.

One of the most interesting results in this study was the high variability of glial changes in different areas of the spinal cord. The distribution of astrocytes varied in different areas of spinal cord, with the highest density of astrocytes in an area of the CC. Different levels of S100B were also observed, especially for the gray and white matter. High spatial variability in astrocyte density, cell shape, and GFAP/S100B expression has also been shown in the brain (Emsley and Macklis, 2006). To the best of our knowledge, this is the first detailed analysis of astrocyte heterogeneity in the spinal cord.

Importantly, Olig2+ cells were also unequally distributed throughout the spinal cord, with high densities observed in the VH and CST. Finally, we also observed changes in glial cell distributions in the gray and white matter of the spinal cord. In summary, our data describing the decreased white matter area, destroyed myelin sheath, decreased levels of specific proteins, changes in levels of myelin-related mRNAs, and increased pool of Olig2-immunopositive cells supported the hypothesis that poor myelinization of the spinal cord is one of the leading components in the pathogenesis of hypogravity motor syndrome. However, we cannot exclude the possibility that the HUM exposes mice to stress, thereby resulting in changes in glial cell distributions and the observed results.

Indeed, recent evidence has suggested that stress can cause activation of astrocytes (Araya-Callís et al., 2012) and microglia (Hinwood et al., 2013), and therefore, we have questioned the adequacy of the HUM as a model reproducing the conditions of weightlessness. The answer to this question can be found by comparing the obtained data with data from studies of the reactions of glial cells in the mouse spinal cord during space flight.

Acknowledgments—This work was supported by grants from RFBR – Russia (12-04-00294, 13-04-00310) and a Presidential grant for government support of the leading scientific schools from the Russian Federation (64631.2010.7). This work was also funded in part by the Russian Ministry of Science and Education (agreement No. 02.A03.21.0002) to support the Program of Competitive Growth of Kazan Federal University.

REFERENCES

Allaman I, Bélanger M, Magistretti PJ (2011) Astrocyte–neuron metabolic relationships: for better and for worse. J Trends Neurosci 34:76–87.

Araya-Callís C, Hiemke C, Abumaria N, Flugge G (2012) Chronic psychosocial stress and citalopram modulate the expression of the glial proteins GFAP and NDRG2 in the hippocampus. Psychopharmacology (Berl) 224:209–222.

Badylak SF, Freytes DO, Gilbert TW (2009) Extracellular matrix as a biological scaffold material: structure and function. Acta Biomater 5:1–13.

Barreto GE, Gonzalez J, Torres Y, Morales L (2011) Astrocytic-neuronal crosstalk: implications for neuroprotection from brain injury. J Neurosci Res 71:107–113.

Brozzi F, Arcuri C, Giambanco I, Donato R (2009) S100B Protein regulates astrocyte shape and migration via interaction with src kinase: implications for astrocyte development, activation and tumor growth. J Biol Chem 284:8797–8811.

Caiozzo VJ, Haddad F, Baker MJ (1996) Microgravity-induced transformations of myosin isoforms and contractile properties of skeletal muscle. J Appl Physiol 81:123–132.

Chen SK, Tvrdik P, Peden E, Cho S, Wu S, Spangrude G, Capecchi MR (2010) Hematopoietic origin of pathological grooming in Hoxb8 mutant mice. Cell 141:775–785.

DeArmond SJ, Deibler GE, Bacon M, Kies MW, Eng LF (1980) A neurochemical and immunocytochemical study of P2 protein in human and bovine nervous systems. J Histochem Cytochem 28:1275–1285.

Donato R, Cannon BR, Sorci G, Riuzzi F, Hsu K, Weber DJ, Geczy CL (2013) Functions of S100 proteins. Curr Mol Med 13:24–57.
Emsley JG, Macklis JD (2006) Astroglial heterogeneity closely reflects the neuronal-defined anatomy of the adult murine CNS. Neuron Glia Biol 3:175–186.
Fitts RH, Trappe SW, Costill DL (2010) Prolonged space flight-induced alterations in the structure and function of human skeletal muscle fibres. J Physiol 88:3567–3592.
Fu H, Kesari S, Cai J (2012) Tcf7l2 is tightly controlled during myelin formation. Cell Mol Neurobiol 32:345–352.
Hachem S, Aguirre A, Vives V, Marks A, Gallo V, Legraverend C (2005) Spatial and temporal expression of S100B in cells of oligodendrocyte lineage. Glia 51:81–97.
Hinwood M, Tynan RJ, Charhley JL, Beynon SB, Day TA, Walker FR (2013) Chronic stress induced remodeling of the prefrontal cortex: structural re-organization of microglia and the inhibitory effect minocycline. Cereb Cortex 8:1784–1797.
Holstege JC, de Graaff W, Hossaini M, Cardona Cano S, Jaarsma D, van den Akker E, DesChamps J (2008) Loss of Hoxb8 alters spinal dorsal laminae and sensory responses in mice. Proc Natl Acad Sci USA 105:6338–6343.
Hunter DJ, Macmaster R, Roszak AW, Riboldi-Tunnicliffe A, Griffiths IR, Freer AA (2005) Structure of myelin P2 protein from equine spinal cord. Acta Crystallogr D 61:1067–1071.
Islamov PR, Tyapkina OV, Bukharaeva EA, Yagodina LO, Ibragimova NN, Valiullin VV, Kozlovskaya IB, Nikolsky EE (2007) Choline acetyl transferase expression in spinal motoneurons of rats following tail-suspension. Dokl Akad Nauk 414:1–3.
Islamov RR, Mishagina EA, Tyapkina OV, Shajmardanova GF, Eremeev AA, Kozlovskaya IB, Nikolski EE, Grigorjev AI (2011) Mechanisms of spinal motoneurons survival in rats under simulated hypogravity on the earth. Acta Astronaut 68:1469–1477.
Kettenmann H, Hanisch UK, Noda M, Verkhratsky A (2011) Physiology of microglia. Physiol Rev 91:461–553.
Kozlovskaya IB, Sayenko IV, Sayenko DG, Miller TF, Khusnutdinova DR, Melnik KA (2007) Role of support afferentation in control of the tonic muscle activity. Acta Astronaut 60:285–295.
Kreutzberg GW (1996) Microglia: a sensor for pathological events in the CNS. Trends Neurosci 8:312–318.
Laurent TC, Laurent UB, Fraser JR (1996) The structure and function of hyaluronan: an overview. Immunol Cell Biol 74:1–7.
Mie M, Kaneko M, Kobatake E (2012) Induction of motor differentiation by transduction of Olig2 protein. Biochem Biophys Res Commun 427:531–536.
Morey-Holton ER, Globus RK (2002) Hindlimb unloading rodent model: technical aspects. J Appl Physiol 92:1367–1377.
Morrison HW, Filosa JA (2013) A quantitative spatiotemporal analysis of microglia morphology during ischemic stroke and reperfusion. J Neuroinflamm 10:1–20.
Nguon K, Li GH, Sajdel-Sulkowska EM (2004) CNS development under altered gravity: cerebellar glial and neuronal protein expression in rat neonates exposed to hypergravity. Adv Space Res 33:1375–1380.
Ohira Y, Nomura T, Kawano F, Sato Y, Ishihara A, Nonaka I (2002) Effects of nine weeks of unloading on neuromuscular activities in adult rats. J Gravit Physiol 9:49–59.
Pruitt KD, Tatusova T, Maglott DR (2007) NCBI reference sequences (RefSeq): a curated non-redundant sequence database of genomes, transcripts and proteins. Nucl Acids Res 35:61–65.
Schlegelmilch T, Henke K, Peri F (2011) Microglia in the developing brain: from immunity to behavior. Curr Opin Neurobiol 1:5–10.
Sofroniew MV, Vinters HV (2010) Astrocytes: biology and pathology. Acta Neuropathol 119:7–35.
Taylor CR, Hanna M, Behnke BJ, Stabley JN, McCullough DJ, Davis 3rd RT, Ghosh P, Papadopoulos A, Muller-Delp JM, Delp MD (2013) Spaceflight-induced alterations in cerebral artery vasoconstrictor, mechanical, and structural: implications for elevated cerebral perfusion and intracranial pressure. FASEB J 6:2282–2292.
Tremblay ME, Lowery RL, Majewska AK (2010) Microglial interactions with synapses are modulated by visual experience. PLoS Biol 8:1–16.
Tyapkina OV, Bukharaeva EA, Nikol'skiĭ EE (2006) The influence of hindlimb unloading on the effectiveness of modulation of the mediator secretion via the autoreceptor system. Biofizika 51:827–832.
Trapp BD, Itoyama Y, MacIntosh TD, Quarles RH (1983) P2 protein in oligodendrocytes and myelin of the rabbit central nervous system. J Neurochem 40:47–54.
Trotter J, Karram K, Nishiyama A (2010) NG2 cells: properties, progeny and origin. Brain Res Rev 63:72–82.
Uva BM, Masini MA, Sturla M, Prato P, Passalacqua M, Giuliani M, Tagliafierro G, Strollo F (2002) Clinorotation-induced weightlessness influences the cytoskeleton of glial cells in culture. Brain Res 934:132–139.
Wake H, Moorhouse AJ, Jinno S, Kohsaka S, Nabekura J (2009) Resting microglia directly monitor the functional state of synapses in vivo and determine the fate of ischemic terminals. J Neurosci 29:3974–3980.

(Accepted 2 September 2014)
(Available online 16 September 2014)